Biocompatible and stable magnetosome minerals coated with poly- l -lysine, citric acid, oleic acid, and carboxy-methyl-dextran for application in the magnetic hyperthermia treatment of tumors

Chalani Mandawala, Imène Chebbi, Mickael Durand-Dubief, Raphael Le Fèvre, Yasmina Hamdous, François Guyot, Edouard Alphandéry

Biocompatible and stable magnetosome minerals coated with poly-L-lysine, citric acid, oleic acid, and carboxy-methyl-dextran, for application in the magnetic hyperthermia treatment of tumors.

Chalani Mandawala[1,2], Imène Chebbi[1],Mickael Durand-Dubief[1], Raphael Le Fevre[1,3], Yasmina Hamdous[1,4], François Guyot[2] , Edouard Alphandéry[1,2,]*

[1]Nanobacterie SARL, 36 boulevard Flandrin, 75016, Paris, France

[2]Institut de minéralogie et de physique des Matériaux et de Cosmochimie, UMR 7590 CNRS, Sorbonne Universités, Muséum National d'Histoire Naturelle, Université Pierre et Marie Curie, IRD, 61 rue Buffon, 75005, Paris, France.

[3]Equipe de Paléomagnétisme, Institut de Physique du Globe de Paris, Paris Cité, Université Paris Diderot, UMR 7154 CNRS, 1 rue Jussieu, Paris, France.

[4]Laboratoire d'Imagerie et Modélisation en Neurobiologie et Cancérologie, Campus Universitaire, Bât. 440, 15 rue Georges Clemenceau, 91406 Orsay Cedex, France.

*CORRESPONDING AUTHOR EMAIL ADDRESS:

edouardalphandery@hotmail.com

ABSTRACT

Magnetic hyperthermia, in which magnetic nanoparticles are introduced into tumors and exposed to an alternating magnetic field (AMF), appears promising since it can lead to increased patients life expectancy. Its efficacy can be further improved by using biocompatible iron oxide magnetosome minerals with better crystallinity and magnetic properties compared with chemically synthesized nanoparticles (IONP – Iron Oxide Nanoparticles). To fabricate such minerals, magnetosomes are first isolated from MSR-1 magnetotactic bacteria, purified to remove potentially toxic organic bacterial residues and stabilized with poly-L-lysine (N-PLL), citric acid (N-CA), oleic acid (N-OA), or carboxy-methyl-dextran (N-CMD). The different coated nanoparticles appear to be composed of a cubo-octahedral mineral core surrounded by a coating of various thickness, composition, and charge, and to be organized in chains of various lengths. *In vitro* anti-tumor and heating efficacy of these nanoparticles were examined by bringing them into contact with GL-261 glioblastoma cells and by applying an AMF. This led to a specific absorption rate of 89-196 W/gFe, measured using an AMF of 198 kHz and 34-47 mT, and to a percentage of tumor cell destruction due to nanoparticles exposed to AMF of 10±3 % to 43±3 % depending on the coating agent. It indicated the potential of these nanoparticles for the magnetic hyperthermia tumor treatment.

KEYWORDS

Magnetosomes, magnetotactic bacteria, magnetosome minerals, minerals, magnetic hyperthermia, alternating magnetic field.

INTRODUCTION

For more than a decade, magnetic nanoparticles are widely used for several biomedical applications, (1,2), such as gene, drug and radionuclide delivery, magnetic bio-separation, (3), magnetic resonance imaging, MRI, and for the magnetic hyperthermia treatment of tumors carried out both *in vitro*, (4), (5), and *in vivo* on animals, (6), (7), and humans, (8). This treatment has proven its efficacy for glioblastoma treatment, (9), leading to an average survival time of 13 months following diagnosis, compared with 4 to 6 months with conventional treatments, (Maier-Hoff2007 et Maier-Hoff 2010).

Magnetic hyperthermia is considered as a nontoxic approach to cancer therapy, in which biological tissues are exposed to moderate temperatures of 43°C to 46°C allowing selective destruction of tumor cells, (11). In magnetic hyperthermia, magnetic nanoparticles are usually administered to tumors and heated several times by applying an alternating magnetic field of strength 5-20 mT and frequency 50-200 kHz, (12). Most of the tested nanoparticles are chemically synthesized superparamagnetic iron oxide nanoparticles, SPION, (13). In this study, we introduce another type of iron oxide nanoparticles, which is synthesized by a strain of magnetotactic bacteria, MTB, called MSR-1 *Magnetospirillum gryphiswaldense*. MTB were originally discovered by Salvatore Bellini in 1963, (14), and reintroduced by Richard Blakmore in 1975, (15). MTB synthesize intracellular magnetic nanoparticles, called magnetosomes, whose magnetic moments align parallel to the earth magnetic field, (16). Magnetosomes act as a compass to guide magnetotactic bacteria in the direction of the earth magnetic field, (17). They are made of a crystallized mineral core composed of magnetite (Fe_3O_4), which is surrounded by an organic layer, (18), (19). They are usually organized in chains, preventing their aggregation, a property which is not usually found among chemical nanoparticles. Moreover, due to their sizes of 30 to 120 nm, high level of crystallinity, ferrimagnetic properties, they heat more efficiently than most chemically synthesized nanoparticles under application of high frequency

magnetic fields, (20). The efficacy of magnetosomes isolated from MTB has already been demonstrated and the concept of evidence established on a murine model with breast cancer, (21). However, the previously tested magnetosome suspensions, which did not undergo any specific treatment, contained pyrogenic endotoxins, which need to be removed for further use in a medicinal preparation, (22).

In this article, we describe a method to produce magnetosome minerals, from which the organic layer originating from MTB has been mostly removed, and which thus contains very low endotoxin concentrations while organizing in stable suspensions. In this method, magnetosomes are extracted from MTB and treated chemically to remove most of the organic material surrounding magnetosome minerals. To prevent their aggregation, magnetosome minerals are then coated with the four following biocompatible coating agents, which have already been used for the stabilization of chemically synthesized nanoparticles: i), poly-L-lysine, PLL, (23), ii), citric acid, CA, (24), iii), oleic acid, OA, (25), (26), or, iv), carboxy-methyl-dextran, CMD, (27). The properties of these coated magnetosome minerals, such as endotoxin concentration, coating thickness, possible arrangement in chains, cytotoxicity tested according to ISO 10993-5, *in vitro* heating, internalization and antitumor efficacy under the application of an AMF are examined and compared with those of pyrogenic magnetosome chains directly extracted from magnetotactic bacteria, MC, and Iron Oxide Nanoparticles (IONP), which are chemically synthesized and currently used for the magnetic hyperthermia treatment of cancer, (11,28). We decided to use IONP since: i) they are ferrimagnetic iron oxide nanoparticles similar in composition and magnetic properties to the magnetosomes but with lower values of coercivity and Mr/Ms (valeurs à reprendre de l'article de Raphael?), (Branquinho and al. (2013), Kasten and al (2014), Zadnik and al (2014)), ii) they are commonly used in the study of magnetic hyperthermia (ToryanaBrown). Since coated magnetosomes are intended to be used on humans, we have followed regulatory guidelines (ISO 10993 standards) for the assessment of their biocompatibility.

EXPERIMENTAL

Materials

Iron Oxide Nanoparticles (IONP). IONP (10-00-102), which are starch coated magnetite nanoparticles, were purchased from Micromod Partikeltechnologie, GmbH, Rostock, Germany. We estimated that IONP contain an endotoxin concentration of 140 EU/ml per mg of iron.

Growth of MSR-1 magnetotactic bacteria. *Magnetospirillum gryphiswaldense* strain MSR-1 (DSM6361) was purchased from Deutsche Sammlung von Mikro-organismen und Zellkulturen (Brunswick, Germany). First, MSR-1 cells are deposited on solid activated charcoal agar medium, and incubated at 29 °C under microaerobic conditions during 7 days, (29). Then, several black-brown colonies are collected from the solid agar medium, containing (completer) and are cultivated and amplified at 29 °C under stirring. Cells are then introduced in a 35 L fermentation medium, containing in 1L of medium 118 ml of 85% lactic acid, 18 ml of 25% to 28% ammonia, 2.4 g of magnesium sulfate, 6 g of potassium phosphate, 0.2 ml of propylene glycol, 6 g of yeast extract and 7 ml of mineral elixir (30). Fermentation is carried out at 29-30 °C under agitation at 200 rpm during 5 days. During fermentation, pH is maintained at 6.9 by adding an acidic feeding medium containing an iron source. Growth of magnetotactic bacteria is stimulated by bubbling oxygen in the growth medium. Temperature, agitation speed, pH, feeding pump flow and oxygen concentration, are monitored and adjusted using an EZ controller and a BioXpert software from Applikon Biotechnology.

Magnetosomes isolated from magnetotactic bacteria, MC. After fermentation, MSR-1 cells are concentrated and washed in water using tangential flow filtration. To lyse the bacteria and obtain a suspension containing pyrogenic chains of MC, concentrated MSR-1 cells are resuspended in 5M NaOH, (31), and heated at 60 °C during 2 hours. Then they are sonicated four times in the presence of a solution of PBS 1X at 10 W during 20 sec, to remove all lysis bacterial cells remains (32).

Uncoated magnetosome minerals, N. MC then undergo the following four treatments: (i), they are re-suspended in a solution containing 1% Triton X-100 and 1% SDS and are then heated at 50 °C overnight; (ii), they are mixed in phenol at pH 8 and then heated at 60 °C during 2 hours in a 25 KHz sonicating bath (SB); (iii), they are re-suspended in chloroform and heated at 60 °C during 2 hours; (iv), they are mixed with a 1 M NaOH solution and heated at 60 °C during 1 hour in the SB, (33), (34) to remove all proteins and lipids. After bacterial lysis and each of the five treatments with detergents, magnetosomes are isolated from non-magnetic organic debris using a neodymium magnet. The supernatant is then removed and replaced by a detergent. Uncoated magnetosome minerals labelled N containing a low percentage of residual organic materials are thus obtained. They are autoclaved and stored at -80 °C.

Coated magnetosome minerals, N-PLL, N-CA, N-OA, and N-CMD. Coating procedures are carried out under sterile conditions, using a sterile flow hood. To prepare the different suspensions of coated magnetosome minerals, four different solutions are first prepared containing: i), 300 mg of poly-L-lysine, PLL, hydrobromide powder dissolved in 6 ml of pyrogen-free water, ii), 105 mg of citric acid, CA, monohydrate powder dissolved in 6 ml of pyrogen-free water, iii), 800 mg of oleic acid, OA, in 40 ml of pyrogen-free water, iv), 840 mg of carboxy methyl dextran, CMD, powder dissolved in 12 ml of pyrogen-free water. They are filtered with a polyether sulfone filter of 0.2 µm and their pH values are adjusted at 10.5, 6, 11.5 or 4.1 for the PLL, CA, OA and CMD solutions, respectively. 1.5 mL of a suspension of uncoated magnetosome minerals at 20 mg of iron /ml is then positioned against a neodymium magnet of remanence 1.3 T during 5 minutes. The supernatant is removed and replaced by 6 mL of a PLL solution at 50 mg /ml, 6 mL of a CA solution at 17.5 mg /ml, 7.5 mL of an OA solution at 20 mg/ml, or 6 mL of a CMD solution at 70 mg/ml. The different mixtures are then sonicated in the SB during 5 hours at 37°C for N-PLL, in the SB during 5 hours at 90°C for N-CA, using a sonicating finger at 10 W during 1h30 for N-OA, or in the SB overnight at room temperature for N-CMD. The protocols for obtaining stable nanoparticles with these different coating agents have been adapted from

previously described coating conditions used with chemically synthesized iron oxide nanoparticles: Babic & al. (2008) for N-PLL (35), Kotsmar & al. (2010) for N-CA (36), Jain & al. (2005) and Yang & al. (2009) for N-AO (37,38) and Liu & al. (2011) for N-CMD (39). Protocols resulting from these articles have been modified in order to have a manufacturing process without harmful products. After sonication, the different suspensions of coated magnetosome minerals are centrifuged at 13000 g during 90 minutes, the supernatant is removed and replaced by pure water. A neodymium magnet is then positioned against the tube containing the different suspensions of coated magnetosome minerals, the supernatant is removed and replaced by pure water.

Characterization of different nanoparticles suspensions

Quantification of iron concentration. To verify total iron concentration of each nanoparticle suspension, nanoparticles are first mixed with a 12 N hydroxide chloride and hydrogen peroxide to produce Fe^{3+} ions complexed with 2 moles per liters of potassium thiocyanate. Iron concentration is then measured at 476 nm with a spectrophotometer (UviLine 9400 Secomam).

Transmission electron microscopy (TEM). To determine the morphology, size, dispersion of the different nanoparticles, 5 µL at 100 µg/ml of each nanoparticle suspension mixed in water are deposited on top of a carbon-coated copper grid (300 mesh from Oxford instruments). They are dried at room temperature and examined using a JEOL JEM-2100 apparatus using a LaB6 gun operated at 200kV. Nanoparticle size and size distribution are estimated by measuring nanoparticle diameters on 500 nanoparticles using the Image J software.

Nanoparticle stability in suspension. The colloidal stability of each nanoparticle suspension is evaluated using 1 mg of a homogenized nanoparticle suspension mixed in 1 ml of water and placed in a quartz cuvette. The variation of the absorption of nanoparticle suspensions with time is measured at 476 nm during 20 minutes using a UviLine 9400 Secoman spectrophotometer. The preparation was carried out two days before the first stability measurement. For each nanoparticle suspension, the stability

measurements are the sum of the measurements carried out during each day within 1 month on three batches of nanoparticles (triplicates). The measurements are performed during 20 minutes after manual shaking. Data are averages of three different measurements.

Zeta potential measurements. Electrokinetic potential or Zeta potential, related to nanoparticle surface charge, is measured at 25°C using a Zetasizer Nano ZS from Malvern Instruments for each type of nanoparticle dispersed in water, at a pH, which is varied between 2 and 12 using a NaOH or HCl solution. Results are averages of three different measurements.

FT-IR measurements. Fourier transform infrared (FT-IR) spectra are measured on lyophilized powders containing the different nanoparticles using a Bucker Vertex 70 ATR Pike Germanium. Each sample spectrum has a 1 cm^{-1} resolution and is obtained for wavenumbers varied between 4000 and 400 cm^{-1}.

CHNS measurements. A CHNS elemental analyzer (Flash 2000 CHNS Analyzer, Thermo Scientific) is used to determine the carbon and nitrogen contents of each lyophilized nanoparticle suspension, containing 3 mg of iron of the different nanoparticle suspensions. Data are averages of three measurements.

***Limulus amebocyte* lysate (LAL)** assay used to estimate endotoxin concentrations in nanoparticle suspensions. This assay is carried out on each nanoparticle suspension to determine endotoxin concentrations, using a Pierce LAL Chromogenic Endotoxin Quantitation Kit (88282 ThermoScientific). 1 ml of each suspension is washed with pyrogen-free water and heated at 70°C over 10 minutes to denature any residual protein that could interfere with the LAL assay. 25 µl of each suspension containing 10 µg in iron are introduced in a 96-well and maintained at 37 °C during the experiment. 25 µl of the LAL solution are added to initiate the reaction. After 10 minutes of reaction, 50 µl of the chromogenic substrate are added to the well during 6 minutes and the amount of endotoxins is detected. Finally, 25 µl of acetic acid are added to stop the reaction. The optical density of the obtained

suspension is measured at 405 nm using a microplate reader. The endotoxin concentration is then estimated using the calibrating curve provided with the kit. To verify that the LAL test does not interfere with the nanoparticles, a recovery rate, defined as $C_{total}/(C_1+C_2)$ is measured, where C_{total} is the endotoxin concentration of the nanoparticle suspensions mixed with a known amount of endotoxin of 0.5 UE/mL, C_1 being the concentration of endotoxins in the different suspensions of nanoparticles and C_2 = 0.5 UE/mL. The estimated recovery rate during the different steps is lower than 50%, indicating that the nanoparticles did not interfere with LAL test. Data are averages of three measurements.

Cell culture

Mouse (GL-261) and Rat (RG2) glioblastoma cells GL-261 cells were purchased from NCI-Frederick (Sample number: 0507812) and cultured in RPMI 1640 medium with L-glutamine (Hyclone) supplemented with 20% of Foetal Bovine Serum (Gibco) and 1% with streptomycin-penicillin solution (10 units penicillin; 10 µg /ml of streptomycin from Hyclone), at 37°C in 5% CO_2. Rat glioblastoma cells (RG2) were purchased from ATCC (CRL-2433) and cultured in DMEM medium (Hyclone) supplemented with 10% of Foetal Bovine Serum (Gibco), 0.11 g/L of sodium pyruvate (Hyclone), penicillin G sodium (50 units /ml from Hyclone) and 50 µg/ml of streptomycin sulfate (Hyclone) at 37°C in 5% CO_2.

Mouse fibroblast cells, BALB/c 3T3 clone 31 (3T3). 3T3 cells were purchased from ATCC (CCL-163) and cultured in DMEM medium (Hyclone) supplemented with 5% of Newborn Calf Serum (Hyclone), 4 mM of L-glutamine, 0.5 mL of streptomycin-penicillin solution (10 units penicillin; 10 µg /ml of streptomycin from Hyclone), and 20 mM of 1M HEPES (Hyclone), at 37°C in 5% CO2. For all experiments, confluent cell monolayers are trypsinized with 0.25% Trypsine-EDTA (Gibco).

***In vitro* cytotoxicity assay of the different nanoparticles.**

Neutral red uptake (NRU) assay according to ISO10993-5. Cytotoxicity of different nanoparticles is determined using the NRU assay on healthy BALB/c 3T3 cell lines according to the protocol described in the standard ISO 10993-5. This assay is based on the accumulation of the neutral red dye in the lysosomes of viable cells. 1.10^4 cells per well are seeded in a 96-well plate and incubated overnight at 37°C in 5% CO_2. The following day, the culture medium is removed and replaced by 100 µl of complete medium with different nanoparticle and iron concentrations of 15.6, 31.2, 62.5, 125, 500, or 1000 µg/ml; cells are incubated at 37°C in 5% CO2 during 24 hours. Then, cells are washed once with a solution containing 150 µl of PBS with calcium and magnesium chloride. 100 µl of a Neutral Red solution at 50 µg/ml is added to the cells and incubated during 3 hours at 37°C in 5% CO_2. Following exposure to 3T3 cells, cells are washed again with 150 µl of PBS and 150 µl of Neutral Red desorbing fixative (glacial acetic acid solution: ethanol: water ; 1%: 50%: 49%) is added followed gentle shaking for 10 min to complete dissolution. Absorbance at 540 nm is measured using a Multiskan FC microplate reader. The percentage of cells inhibition (% Inhibition), is calculated using the formula: $\%\ \text{Inhibition} = \left(1 - \left(\frac{\text{DO}_{\text{sample}}}{\text{DO}_{\text{control}}}\right)\right) \times 100$, where $\text{DO}_{\text{sample}}$ is the absorbance of cells with nanoparticles and $\text{DO}_{\text{control}}$ is the absorbance of cells only. These experiments are carried out in triplicate.

MTT assay. Cytotoxicity of different nanoparticles on GL-261 and RG2 cell lines is determined using the MTT (3-(4, 5-dimethylthiazol-2-yl)-2, 5-diphenyltetrazolium bromide) assay. 5.10^3 cells per well are seeded in a 96-well plate and incubated overnight at 37°C in 5% CO_2. The following day, the culture medium is removed and replaced by 100 µl of complete medium with different nanoparticle and iron concentrations of 15.6, 31.2, 62.5, 125, 500, or 1000 µg/ml; cells are incubated at 37°C in 5% CO_2 during 72 hours. Then, cells are washed once with a solution containing PBS with calcium and magnesium chloride. 100 µl of a MTT solution at 1 mg/ml is added to the cells and incubated during 2 hours at 37°C in 5% CO_2. The MTT solution is carefully removed and replaced by 100 µl of an isopropanol solution. The plates are mixed thoroughly to dissolve purple formazan crystals and incubated at 37 °C during 4 hours to ensure that all crystals are dissolved. Then the optical density

representing the viable cell number resulting from the solubilized purple formazan is estimated at 540 nm using a Multiskan FC microplate reader. And the percentage of cells inhibition (% Inhibition), is calculated from the formula: $\%\ \text{Inhibition} = \left(1 - \left(\frac{\text{DO}_{\text{sample}}}{\text{DO}_{\text{control}}}\right)\right) \times 100$, where $\text{DO}_{\text{sample}}$ is the absorbance of cells with nanoparticles and $\text{DO}_{\text{control}}$ is the absorbance of cells only. These experiments are carried out in triplicate. To get rid of the interference between the MTT assay and the nanoparticles, we subtracted the value of the optical density of the assembly containing cells and nanoparticles to the value of the optical density obtained after adding MTT to the assembly. The same protocol was followed with Neutral Red.

***In vitro* nanoparticle antitumor and heating efficacies as well as nanoparticle cellular internalization in the presence of the AMF.**

Magnetic hyperthermia set-up. In an attempt to get close to *in vivo* treatment conditions, the magnetic hyperthermia experimental set-up was not adiabatic. We used an induction system and a coil of 7 cm to expose the mixture of cells and nanoparticles to an alternating magnetic field (AMF) of 34-47 mT and 198 kHz.

Hyperthermia treatment with AMF. *In vitro* studies are carried out using 1 mg in iron of the different nanoparticle suspensions brought into contact with GL-261 cells and exposed during 30 minutes to an alternating magnetic field of 198 kHz and strength of 34 to 47 mT. 2.5 10^5 GL-261 cells are seeded in a 35 mm Petri dish and incubated for 24 hours at 37°C in 5% CO_2. After 24 hours, the culture medium is removed and replaced by 2 ml of complete medium with or without 1 mg (concentration = 0.5 mg/mL et pas 1 mg/mL ?) of the different nanoparticles. Samples are then, or not for the control, exposed during 30 minutes to either one of the following two magnetic treatments. In the first magnetic treatment, temperature is maintained at 43°C - 46°C by applying an alternating magnetic field of frequency 198 kHz and strength adjusted manually between 34 and 47 mT. In the second one, an alternating magnetic

field of 198 kHz and strength 34 mT is applied. The temperature is measured by the infrared camera (ThermoPro^{TM} EasIR-2 Thermal Imager) and infrared images are analyzed by the provided analyzer software.

The second magnetic treatment is used to measure the specific absorption rate (SAR), measured in Watt per gram of iron, of the different nanoparticles mixed with GL-261 cells. SAR is estimated using the formula: $SAR = C_{water} . \left(\frac{\delta T}{\delta t}\right) . \left(\frac{1}{C_{iron}}\right)$, where C_{water} = 4.2 J/(g.K) is the specific heat capacity of water, $\Delta T/\delta t$, measured in °C/s, is the initial slope of the temperature variation with time and $C_{iron,}$ measured in g of iron per g of water, is the iron concentration in the different nanoparticle suspensions. The choice of these parameters seems accurate since heat capacities of culture medium and water are similar, (ref), and nanoparticle concentrations do not change significantly when nanoparticles are mixed in culture medium (vérifier). Data are averages over three measurements.

Flow cytometer measurements. Following these two magnetic treatments, cells are washed once with a solution containing PBS with calcium and magnesium, and incubated during 24h with 2 ml of complete medium at 37°C in 5% CO_2. In order to harvest cells, the culture medium is removed and replaced by 500 µl of Trypsin-EDTA. 2 ml of complete medium are added to neutralize Trypsin-EDTA and to obtain a cell suspension whose cell viability is measured with a flow cytometer. Before and after one magnetic treatment, the percentage of living cells is estimated. For that, 5 µL of 20 mg /ml of propidium iodide (PI) is introduced in 500 µl of a GL-261 tumor cell suspension mixed with the different nanoparticles. A Flow cytometer (Beckton Dickinson FACS Calibur 3C, BD Biosciences) is used to excite PI with an argon laser at 488 nm and to detect PI emission with a FL3-H detector. PI, which only penetrates in inactivated cells, is used to estimate the percentage of inactivated cells. Twenty thousand cells per sample were measured to determine the percentage of living cells.

Internalization of nanoparticles. Before and after one magnetic treatment, the quantity of iron of nanoparticles internalized in GL-261 cells is also measured. GL-261 tumor cells are first washed

279 twice with PBS to remove nanoparticles from cell surface and it is verified by optical microscope
280 observation that nanoparticle aggregates do not remain at the cell surface and that the quantity of iron
281 actually mainly corresponds to the quantity of iron internalized in cells, whether it corresponds to
282 crystallized or dissolved iron. 500 µl of GL-261 tumor cells are collected for cell counting and 1 ml of
283 each cell suspension is used to measure the quantity of iron contained per cell. For that, cell suspensions
284 are first centrifuged at 13000g during 10 minutes. The supernatant is removed and the cell pellet
285 containing cells and nanoparticles is re-suspended with 250 µl of $HCl:HNO_3$ (3:1) solution and
286 incubated overnight. This $HCl:HNO_3$ (3:1) solution dissolves crystallized iron oxide into Fe^{2+} and Fe^{3+}
287 ions and denatures cell membranes. 50 µl of each sample are mixed with 50 µl of HCl (6N), 50 µl of
288 H_2O_2 (20%) and 50 µl of potassium thiocyanate (2M). This mixture induces the formation of a complex
289 between iron (III) and thiocyanate ions. Measurement of iron internalized in cells is estimated by
290 measuring the concentration of this complex by absorption at 476 nm. Hyperthermia treatments and
291 internalization studies were carried out without washing cells following nanoparticle incubation in the
292 first case and with washing cells following nanoparticle incubation in the second case. In this way, we
293 could study nanoparticle toxicity towards cells as well as nanoparticle cellular internalization in the
294 presence of AMF.

295

RESULTS AND DISCUSSION:

To produce a magnetosome suspension, which can be used as a medicinal product, four steps are followed: i), MSR-1 magnetotactic bacteria are first cultivated, ii), pyrogenic magnetosomes chains are then extracted from these bacteria, called MC, iii), MC are purified to yield a suspension of magnetosome minerals, called N, which only contains a small quantity of organic material coming from these bacteria, iv), magnetosome minerals are then coated with PLL, CA, OA, and CMD to produce four different coated magnetosome minerals, called N-PLL, N-CA, N-OA, and N-CMD, respectively.

Characterization of samples containing uncoated magnetosome minerals extracted from whole MSR-1 magnetotactic bacteria and purified

MSR-1 magnetotactic bacteria, which are used in this study to produce magnetosomes, are characterized using transmission electron microscopy (TEM). When 5 µl of a suspension containing these bacteria are deposited on top of a carbon-thin-film-covered grid, dried and observed by TEM, Fig.Fig. 1(a) shows that each bacterium typically contains a long chain of 30 magnetosomes, (Faivre2008).). Despite of better heating properties compared to their chemical counterparts, (20), (40), magnetosomes from MTB are not currently used as a medicinal product, most probably due to the presence of endotoxins, including lipopolysaccharides, which could contaminate magnetosome medicinal preparations. Since magnetosome formation results from the invagination of the bacterial membrane, (40), endotoxin concentration at magnetosome surface might be higher than the tolerated concentration.

In this study, MC are therefore extracted from magnetotactic bacteria with NaOH and then treated with a series of different detergents (SDS, Triton X100, phenol and chloroform) at a temperature of 60°C in the presence of sonication to remove most of the organic material, including endotoxins, coming from MSR-1 magnetotactic bacteria. Uncoated magnetosome minerals are thus obtained and characterized.

When 2 µl of a suspension of uncoated magnetosome minerals are deposited on top of a carbon grid and observed by TEM, no remains of organic material remain visible (Fig.1(c)). These uncoated magnetosome minerals aggregate strongly and have a mean size of 43 nm (Fig. 2(a)), which is larger than that of 21 nm, observed for IONP (Fig. 1(b)). Treatments involved in magnetosome extraction and purification did not significantly modify magnetosome morphology and size, with reference to those observed in whole magnetotactic bacteria. The FT-IR spectrum of a lyophilized suspension of uncoated magnetosome minerals, presented in Figure 3(a), shows two dominant peaks attributed to iron oxide at 609 cm^{-1} and 673 cm^{-1}, (42). When they are contained inside magnetotactic bacteria, magnetosome iron oxide composition consist of magnetite,(43). After extraction and purification, saturating isothermal remanent magnetization (SIRM) measurements, carried out on uncoated magnetosome minerals, reveal a maghemite composition, (44). Additional peaks observed in FT-IR spectra at 1041 cm^{-1}, 2926 cm^{-1}, and 3267 cm^{-1}, (Fig.3(a)), are attributed to PO, C-H, NH_2 and OH vibrational modes, respectively. These signals are due to residual organic material remaining at the magnetosome mineral surface after purification. The quantity of this organic material is further estimated by CHNS measurements carried out on a homogenized lyophilisate of uncoated magnetosome minerals. These measurements reveal the presence of 2.39 ± 0.04% of carbon residue coming from whole magnetotactic bacteria in 1 mg of uncoated magnetosome minerals (Fig. 2(b)). Concerning the endotoxin concentration in the suspension of uncoated magnetosome minerals, it lies between 10 and 160 EU /ml per mg of iron as estimated by a LAL test. This indicates that uncoated magnetosome minerals are much less pyrogenic than suspensions of whole magnetotactic bacteria, characterized by endotoxin concentrations larger than 1.10^5 EU /ml per mg of iron, and then suspensions containing MC extracted from magnetotactic bacteria by a unique NaOH treatment, which possess endotoxin concentrations lying between 2000 and 12000 EU /ml per mg of iron. However, uncoated magnetosome minerals tend to aggregate as revealed by TEM image shown in Figure 1(c), and by absorption measurements at 480 nm of a suspension containing 1 mg /ml in iron of uncoated magnetosome minerals. Their absorption signal decreases rapidly by 80% in 20 minutes (Fig. 2(c)). Moreover, the variation of the surface charges of these uncoated magnetosome

minerals as a function of pH is shown in Fig. 2(e). It shows a zeta potential increase from -15 mV to 0 mV between pH 5 and 6 followed by a zeta potential decrease from 0 to -20 mV between pH 6 and 7. Such a large variation in zeta potential, observed within a relatively narrow range of pH, could be explained by magnetosome aggregation, which is believed to be dependent on surface charge, (21). Zeta potential with measurements of the surface charge make it possible to establish the degree of interaction between nanoparticles, in our example a significant variation in the surface charge would indicate nanoparticles more or less aggregated devoid largely of the layer of original biological material. For medical applications, it is essential to use suspensions that are stable since aggregation can lead to embolism *in vivo*, and can also prevent a thorough magnetosome administration and a uniform magnetosome heat production.

Characterization of suspensions containing coated magnetosome minerals

Administration to an individual of a magnetosome suspension requires the use of a stable suspension. To achieve this aim, magnetosome minerals are coated with PLL, CA, OA, or CMD, chosen for their good solubility in water, biocompatibility and low toxicity, (35–39)
. TEM measurements carried out on suspensions containing the four different coated magnetosome minerals, N-PLL, N-CA, N-OA, N-CMD, respectively deposited on carbon grids for TEM observations (Figs. 1(d) to 1(k)) which reveal the presence of a coating material surrounding magnetosome mineral cores with average thicknesses between 4 and 6 nm for N-PLL, 2 and 5 nm for N-CA, 3 and 5 nm for N-CMD and lower than 2 nm for N-OA. TEM images of Figures 1(d) to 1(k) show that N-PLL, N-CA, N-OA, and NCM-D are arranged in chains with preferential crystallographic common orientations, as presented elsewhere, (ref), and demonstrated for magnetosomes directly extracted from AMB-1 magnetotactic bacteria, (44). Chemically synthesized iron oxide nanoparticles are rarely reported to organize in chains. When an organization in chains of such nanoparticles is described, (45), their behavior contrasts with that observed with coated magnetosome minerals. Indeed, chemically synthesized nanoparticles do not appear to have preferential alignments and are usually

superparamagnetic. FT-IR spectra of lyophilized suspensions of N-PLL, N-CA, N-OA and N-CMD, provide further support for the presence of the various coating agents at the magnetosome mineral surfaces. For N-PLL, peaks at 1546 cm^{-1}, 1651 cm^{-1} and 3266 cm^{-1} are attributed to the NH, C=O and NH_2 bonds of poly-L-lysine respectively (Fig. 3(c)). Concerning N-CA, the peaks at 1631 cm^{-1} and 3250 cm^{-1} are due to C=O and OH bonds of citric acid (Fig. 3(d)). Regarding N-OA, the peaks at 1427 cm^{-1}, 1546 cm^{-1} and 3250 cm^{-1} are attributed to C-O, C=O and OH bonds of oleic acid (Fig. 3(e)). Similarly, for N-CMD, the peaks at 1034 cm^{-1} and 3250 cm^{-1} arise from the C-O and OH bonds of carboxy-methyl-dextran. CHNS measurements, carried out on lyophilized suspensions of N-PLL and N-OA show a percentage of carbon of 4.91 ± 0.09% and 8.16 ± 0.02 % respectively, which is higher than that of 2.39 ± 0.04%, which is estimated for uncoated magnetosome minerals (Fig. 2 (b)). This result suggests that in N-PLL and N-OA coating material is added to mostly uncoated magnetosome minerals. By contrast, for N-CA and N-CMD, CHNS measurements reveal a percentage of carbon of 2.41 ± 0.16% and 2.37 ± 0.02%, which is similar to that estimated for uncoated magnetosome minerals. In N-CA and N-CMD, it is therefore possible that residual organic material at the surface of uncoated magnetosome minerals has been replaced by the coating material. The presence of coating in nanoparticles mixed in suspension can also be observed from zeta potential measurements, which indicate that N-CA, (35), N-OA, (46), and N-CMD, (38), are negatively charged at pH 7, a behavior which could be due to the presence of carboxylic and hydroxyl functional groups at the surfaces of N-CA, N-OA, or N-CMD (Figs. 2(e) and 2(f)), while N-PLL appear positively charged at pH 7, a property that could come from the presence of a tertiary amine function (pKa of PLL = 10.5) at N-PLL surface (Fig. 2(e)). By contrast to uncoated magnetosome minerals, all four coated magnetosome minerals appear to be stable in suspension. Indeed, the absorption of homogenized suspensions containing 1 mg/ml of N-PLL, N-CA, N-OA and N-CMD, measured at 480 nm, decreases by less than 40% in 20 minutes (Figs. 2(c) and 2(d)). The magnitude of this absorption decrease is comparable to that observed for stable chemically synthesized nanoparticles IONP. Coating therefore leads to well dispersed N-PLL,

N-CA, N-OA and N-CMD, as shown in the TEM images presented in Figures. 1(e, g, i, k) and confers stability to the four different coated magnetosome minerals suspensions in water. Therefore, administration of these suspensions to human, which usually requires less than 20 minutes, seems feasible. The biocompatibility of these nanoparticles is first demonstrated using an LAL assay, which shows that the endotoxin concentration of N-PLL, N-OA, N-CA, and N-CMD suspensions is 21-160 EU/ml per mg of iron for N-PLL, 20-130 EU/ml per mg of iron for N-CA, 10-105 EU/ml per mg of iron for N-OA, 23-140 EU/ ml per mg of iron for N-CMD. These concentrations are lower than 160 EU/ml per mg of iron, an endotoxin concentration comparable to that of 140 EU /ml per mg of iron, measured for chemically synthesized nanoparticles, IONPs.

Cytotoxicity of the different nanoparticles towards healthy 3T3 cells in the absence of magnetic treatment

Their biocompatibility is further determined following ISO 10993 standards. Such standards are followed since uncoated and coated magnetosome mineral are both considered as medical devices given that their dominant mode of action does not involve any immunological, pharmacological or metabolic effect but only heat. Cytotoxicity of suspensions containing various concentrations of IONP, uncoated and coated magnetosome minerals, *i.e.* between 16 µg/mL and 1 mg/mL, is estimated on healthy 3T3 cells using a NRU assay according to ISO 10993-5 standard. ISO 10993-12 recommends using a concentration of 6 cm^2/ml for medical devices with a high surface to volume ratio such as nanoparticles, corresponding to 22 µg /ml for magnetosomes, (47) .Therefore the tested concentration range includes concentrations that are above the concentration of 6 cm^2/ml recommended by ISO 10993-12. 3T3 cell viability is measured after cellular incubation in the presence of the different nanoparticles during 24 hours. Figure 4(a) shows the percentage of 3T3 cell inhibition as a function of nanoparticle concentration, measured in mg of iron per ml. When 3T3 cells are brought into contact with IONP, N, N-PLL, N-CA, N-OA and N-CMD, Figure 4(a) shows that the average percentage of cell inhibition remains below ~ 30%, suggesting that the different nanoparticles are not cytotoxic below 1 mg per ml

according to the criteria of ISO 10993-5 standard. These experiments also indicate that inhibitory concentrations leading to 50% cell inhibition, IC_{50}, of the different nanoparticles are high and larger than 1 mg per mL, indicating that these different nanoparticles are not cytotoxic towards healthy 3T3 cells at these tested nanoparticle concentrations.

Cytotoxicity of the different nanoparticles towards glioblastoma GL-261 and RG-2 cells in the absence of magnetic treatment

Cytotoxicity of suspensions containing IONP, uncoated and coated magnetosome minerals, is further evaluated on glioblastoma GL-261 and RG2 cells using a MTT assay. Percentage of cell inhibition is estimated as a function of the different nanoparticle concentrations, varied between 15.6 µg per mL and 1 mg per mL, after nanoparticle incubation during 24 hours with GL-261 (Figure 4(b)) or RG2 (Figure 4(d)) cells. Uncoated iron oxide particles display low cytotoxicity towards 3T3, GL-261 and RG2 cells, with a percentage of cell inhibition remaining below 20% for all tested concentrations in Figures 4(a), 4(b) and 4(d). As observed with IONP, N-PLL and N-CA reach a larger than 30% percentage of cell inhibition at 1 mg/mL and appear as observed with IONP to be more cytotoxic towards GL-261 and RG2 cells than towards 3T3 cells (Figures 4(a), 4(b) and 4(d)). By contrast, Figures 4(a), 4(b), and 4(d), show that N-OA are less cytotoxic towards GL-261 and RG2 cells than towards 3T3 cells. N-CMD display a rather unusual behavior with significant cytotoxicity towards 3T3 and RG2 cells (Figure 4(a) and 4(d)) and low cytotoxicity towards GL-261 cells (Figure 4(b)). IC_{50} values on GL-261 and RG2 cells, respectively of 269 and 355 µg /ml for N-PLL, 606 and 733 µg /ml for N-CA, larger than 1 mg /ml and 919 µg /ml for N-CMD, and larger than 1 mg /ml for uncoated magnetosomes, N-OA and IONP. In the absence of AMF application, optimal coating materials, which may correspond to those leading to the largest cytotoxicity towards tumor cells and to the lowest cytotoxicity towards healthy cells, may therefore be poly-L-lysine and citric acid.

After 72 hours of incubation of the different nanoparticles, the percentage of cell inhibition is

measured as a function of nanoparticle concentration, varied between 15.6 µg /ml and 1 mg /ml, on GL-261 (Figure 4(c)) and RG2 (Figure 4(e)) cells. Compared with 24 hours, the cytotoxicity is enhanced at 72 hours, leading to IC50 values, on GL-261 and RG2 cells, respectively larger than 1 mg /ml for N, 653 and 672 µg /ml for N-CMD, 271 and 433 µg /ml for N-CA, 224 µg /ml, and more than 1 mg /ml for IONP, 271 and 303 µg /ml for N-OA, and 6 and 197 µg /ml for N-PLL, respectively. IC_{50} values are lower towards GL-261 cells than towards RG2 cells. Given that cytotoxicity towards tumor cells is increased with incubation time, magnetic hyperthermia treatment efficacy may not decrease when nanoparticles stay in the tumor.

Cytotoxicity of the various coated magnetosome minerals on GL-261 cells without AMF is due to the coating since uncoated magnetosome minerals are characterized by an absence of cytotoxicity. It could be explained on the one hand by cytotoxic properties of the coating agents surrounding the magnetosome minerals (Suppl. Fig. 1 (a)) and on the other hand by variations in dispersion properties of the magnetosome minerals, as a function of their coatings, (23). Compared with commonly used cytotoxic cancer drugs characterized by IC_{50} values of 16.3 ng /ml for doxorubicin, (48), 4.1 µg /ml for tamoxifen, (48), 22 to 56 ng /ml for cisplatin, (49), and 96 to 120 ng /ml for carboplatin, (49), N-OA, N-CA, N-CMD, and N-PLL, possess much higher IC_{50} values. By contrast to conventional cytotoxic cancer drugs, the main mode of action involved in tumor cell destruction using magnetic hyperthermia with N-OA, N-CA, N-CMD, and N-PLL, thus does not come from their cytotoxicity, which would require much lower IC_{50} values. Instead it comes from heat generated by AMF application.

Cell destruction, internalization, heating properties of the different nanoparticles in the presence of glioma GL-261 cells under alternative magnetic field application.

To measure the specific absorption rate (SAR) of IONP, uncoated and coated magnetosome minerals, 1 mg/mL in iron of these different nanoparticles is brought into contact with GL-261 cells during 24 hours and then exposed during 30 minutes to an alternating magnetic field of frequency 198

kHz and average field strength of 34 mT. The variation with time of the average spatial temperature distribution over the whole Petri dish containing the cells mixed with the various nanoparticles is presented in Figure 5(a). From the initial slopes of the plots of Figure 5(a), 0.018 °C/sec. < $\Delta T/\delta t$ < 0.047 °C/sec., average SAR are estimated as ~ 96 W/gFe, ~ 73 W/gFe, ~ 89 W/gFe, ~ 141 W/gFe, ~ 100 W/gFe, ~ 196 W/gFe for N, IONP, N-PLL, N-CA, N-OA, and N-CMD, respectively (Table 1). After 30 minutes of application of the alternating magnetic field, the maximum temperatures reached are measured as 39.4 °C, 35.0 °C, 33.7 °C, 41.8 °C, 42.3 °C and 50.8 °C for N, N-PLL, N-CA, N-OA, and N-CMD, respectively. In petri dishes, N-CMD, N-CA and N-OA lead to higher SAR values and maximum temperatures as well as to a more homogenous temperature distribution, where the latter may be defined as the temperature distribution that yields the largest percentage of heated area at 43-46 °C (table 2), a range of temperature that is reported to produce antitumor efficacy in hyperthermia treatment, (ref montrant que l'hyperthermie a lieu pour des temperatures de chauffage supérieures à 43-46 °C), compared with uncoated magnetosomes. The opposite behavior is observed for N-PLL having smaller SAR values and yielding smaller maximum temperatures and less homogenous temperature distribution than uncoated magnetosomes (Fig. 5(b)). This difference in behavior may be explained by different thicknesses and properties of the coatings. Indeed, as observed in the TEM image of Fig. 1(e), the largest coating thickness of 6.4 nm and possible changes in magnetosome morphology and chain length, observed in N-PLL, leads to the lowest heating rates. Assuming that Brown relaxation is occurring within these large nanoparticles as previously reported, (ref à trouver), the presence of such thick coating could decrease N-PLL rotation motions or friction with the viscous surrounding, hence minimizing the amount of heat produced. By contrast, magnetosome minerals with a thin coating seem to heat more, possibly due to better thermal conductivity. Optimal coating thickness, leading to enhanced heat production, appear to lie between 2 and 4.5 nm as is the case for N-CA, N-OA and N-CMD and is close to the coating thickness of ~6 nm of magnetosomes before purification, (ref à rajouter). As a whole, N-PLL, N-CA, N-OA, and N-CMD, all lead to higher SAR values and equivalent

494 or better heat distribution than IONP, suggesting that they all possess promising heating properties to
495 carry out magnetic hyperthermia.

496 Next, we examine how efficiently N, IONP, N-CA, N-PLL, N-CMD, and N-OA can reach *in*
497 *vitro* temperatures of 43- 46°C, which are typical temperatures desired for magnetic hyperthermia, (10:
498 faux). For that, 1 mg of the different nanoparticles is brought into contact with GL-261 cells during 24
499 hours and then exposed, or not for the control, to a heat treatment at 43- 46°C during 30 minutes. Heat is
500 maintained at these temperatures by applying an alternating magnetic field of frequency 198 kHz and
501 average strength of 34-47 mT. While for N-CA, N-OA, and N-CMD, a magnetic field strength of 33 to
502 40 mT is needed to reach an average temperature in the Petri dish of 45°C after 30 minutes of treatment,
503 leading to a more homogenous temperature distribution (Table 2) than for N and IONP (Figure 6(b)), a
504 different behavior is observed for N-PLL that require the application of a higher magnetic field of 47
505 mT to reach an average temperature of 42 °C after 30 minutes of treatment and yield a less homogenous
506 temperature distribution (Table 2) than for uncoated magnetosomes and IONP (Fig. 6(b)).

507 We now turn to a comparison between *in vitro* antitumor efficacy against GL-261 tumors of N-
508 CA, N-PLL, N-CMD, and N-OA, with that of uncoated magnetosomes and IONP. As shown in Figure
509 6(a), for all nanoparticles studied, the percentage of GL-261 living cells decreases in the presence of
510 heat treatment at 43-46 °C. While for N-OA and N-CMD, GL-261 cell destruction appears to be the
511 most efficient, leading to a decrease in the percentage of living cells of 30-40 ±2% following heat
512 treatment, close to that of 53% ± 2.2% observed with IONP, such decrease is only 10-16 ± 2% for N-
513 PLL, N-CA and uncoated magnetosomes, lower than for IONP. For magnetic hyperthermia, it is
514 desirable to use nanoparticles that can induce cell destruction at low magnetic field strength to prevent
515 eddy currents. Therefore, N-OA and N-CMD seem to be the most efficient nanoparticles since their
516 relatively high percentage of cell destruction of 30-40 ±2% is correlated with relatively high
517 temperatures of 52-53 °C reached during 30 minutes of application of a magnetic field of relatively low
518 strength of 33-40 mT (Fig. 6(a)). Although IONP yield a relatively high percentage of cell destruction of

519 53% ± 2.2%, they seem to be less promising since the relatively high temperature of 48 °C that they
520 reach requires the application of an alternating magnetic field of high strength of 47 mT during 30
521 minutes (Fig. 6(b), which may produce Eddy currents resulting in global warming of the whole
522 organism, (Ref. : « Effects of size distribution on hysteresis losses of magnetic nanoparticles for
523 hyperthermia »,Rudolf Hergt, Silvio Dutz and Michael Roder (2008)). N-PLL and uncoated
524 magnetosomes appear to be the less promising nanoparticles since they induce the smallest percentages
525 of cell destruction of 16% ± 2.3%, obtained at relatively low temperatures of 42-48 °C by applying
526 magnetic fields of high strength of 47 mT (Fig. 6(b)).

527 To examine whether *in vitro* antitumor efficacy is due to cellular internalization of the different
528 nanoparticles, N-PLL, N-OA, N-CA, N-CMD, uncoated magnetosomes, and IONP, are exposed to the
529 same heat treatment as above at 43-46 °C. The different nanoparticles are removed from the cell surface
530 by washing and it is verified by optical microscopy that nanoparticle aggregates do not remain at the
531 cell surface, so that the quantity of internalized nanoparticles, whether composed of crystallized or
532 dissolved iron, can be measured. As shown in Figure 7, after heat treatment, the amount of internalized
533 iron either increases from 1 to 4 pg per cell for N-PLL, from 2 to 18 pg per cell for N-CA, or remains
534 relatively unchanged at 0.5 to 4 pg per cell for uncoated magnetosome minerals, N-OA, N-CMD and
535 IONP. High cellular internalization of N-CA in the presence of the heat treatment at 54 °C (Figure 6(b))
536 may possibly be explained by N-CA high affinity for cellular membrane, as it is the case for
537 superparamagnetic nanoparticles coated with citric acid,(50). In the literature, anionic maghemite
538 nanoparticles have indeed been shown to have a high affinity for cellular membrane mainly due to
539 electrostatic interactions, (51). These behaviors may also take place with N-CA and promote their
540 cellular internalization.

541 On the one hand, N-CA that are prone to the highest level of internalization, produce a small
542 decrease in the percentage of GL-261 living cells of only 10% ± 2.8% following heat treatment at 54 °C,

543 which may be due to the relatively limited cytotoxicity of citric acid (IC_{50} ~ 606 µg/ml), (50). This
544 hypothesis is further supported by analyzing the behavior of MC, which internalize and lead to
545 enhanced cytotoxicity following magnetic field application (Suppl. Figs. 1(a) and 1(b)). In this case,
546 cytotoxicity may arise from bacterial residues that enter inside cells following magnetic field
547 application. On the other hand, nanoparticles that appear to yield most efficient cell destruction, *i.e.* N-
548 OA and N-CMD with percentages of cell destruction of 43% ± 2.9% and 30% ± 2.0% respectively, do
549 not internalize much in cells, suggesting that internalization may not be the main factor responsible for
550 nanoparticle cytotoxicity. Instead, *in vitro* antitumor efficacy following alternating magnetic field
551 application may be due to aggregation of nanoparticles at the cell surface, to homogenous heating,
552 mechanic chocks between nanoparticles and cell membranes, or to extracellular hyperthermia, (52),
553 which could result in cell lysis. Chemical nanoparticles coated with OA have already been used to
554 induce toxicity *in vitro* under the application of an alternating magnetic field, (53), reinforcing the idea
555 that N-OA are-suitable for the magnetic hyperthermia treatment of tumors.

556 Coated magnetosome minerals also appear promising for magnetic hyperthermia, since N-PLL have
557 been shown to efficiently destroy both subcutaneous GL-261 and intracranial U-87 glioblastoma tumors
558 under AMF applications, as presented in details elsewhere, (43), (54).

559 **CONCLUSIONS**

560 In this study, we describe a process for purifying iron oxide nanoparticles extracted from
561 magnetotactic bacteria and removing most of the organic material, including endotoxins. The
562 nanoparticles are then stabilized with four different biodegradable and biocompatible coating agents.
563 These coated magnetosome minerals are characterized by a mineral crystallized core composed of
564 maghemite, which is surrounded by a layer of coating agent and are arranged in chains of coated
565 particles. Sedimentation and electro kinetic potential measurements reveal that they have good colloidal
566 stability at physiological pH 7.4, which is a good criterion for injecting nanoparticles into tumor.

Moreover, their endotoxin concentrations are below 160 EU/ml per mg and comparable to that of chemically synthesized nanoparticles IONP. Cytotoxicity assays reveal that the percentage of healthy 3T3 cell inhibition by N-PLL, N-CA, N-OA, and N-CMD at concentrations varied between 16 µg/ml and 1 mg/ml is lower than 30% indicating that, according to ISO 10993-5 standard, these nanoparticles are not toxic. The SAR, measured when these nanoparticles are brought into contact with GL-261 cells and exposed during 30 minutes to an alternating magnetic field of 198 kHz and strength 34 mT, lie between 89 and 196 W/gFe, larger than the SAR of 73 W/gFe, measured for chemically synthesized nanoparticles IONP, currently used to carry out magnetic hyperthermia treatment of tumors. *In vitro* anti-tumor efficacy of N-PLL, N-CA, N-OA, and N-CMD is also examined by bringing them into contact with GL-261 cells and by heating them to 43-46°C under application of an alternating magnetic field of 198 kHz and 34-47 mT. Decrease in the percentage of living GL-261 cells following magnetic heat treatment is the largest for N-CMD and N-OA and the lowest for N-CA and N-PLL. Interestingly, N-CA internalize efficiently in GL-261 cells following magnetic heat treatment, while the opposite behavior is observed for N-CMD and N-OA. Therefore, efficient GL-261 tumor cell destruction does not seem to be correlated with a high level of nanoparticle internalization, but instead with high SAR values of ~ 100-196 W/gFe and with homogeneous heating at the scale of a Petri dish, measured for N-CMD and N-OA. Although IONP yield a significant percentage of cell inhibition in the presence of the AMF, this is achieved by using an AMF of high strength (47 mT), which should be avoided in humans, since it can lead to Eddy currents and global warming of the organism. These results indicate that coated magnetosome minerals are good candidates to carry out the magnetic hyperthermia treatment of tumors. SAR values and *in vivo* biodistribution should both be optimized to produce the most efficient magnetic hyperthermia.

ACKNOWLEDGMENT:

We would like to thank the Eurostars program (Nanoneck-2, E9309), subvention AIR from the region of Paris (A1401025Q) as well as the ANRT (CIFRE 2014/0359). Chalani Mandawala is a PhD student

(CIFRE 2014/0359), working both at Nanobacterie and at the Muséum National d'Histoire Naturelle. Chalani Mandawala carried out the experiments and Edouard Alphandéry directed the research described in this article.

596 **REFERENCES**

597 1. Gupta AK, Gupta M. Synthesis and surface engineering of iron oxide nanoparticles for biomedical
598 applications. Biomaterials. juin 2005;26(18):3995‑4021.

599 2. Giakisikli G, Anthemidis AN. Magnetic materials as sorbents for metal/metalloid preconcentration
600 and/or separation. A review. Analytica Chimica Acta. juill 2013;789:1‑16.

601 3. Pankhurst QA, Connolly J, Jones SK, Dobson J. Applications of magnetic nanoparticles in
602 biomedicine. Journal of Physics D: Applied Physics. 7 juill 2003;36(13):R167‑81.

603 4. Berry, Catherine C, Curtis, Adam S.G. Functionalisation of magnetic nanoparticles for applications
604 in biomedicine. J Phys D: Appl Phys. 2003;36:R198–R206.

605 5. Jordan A, Scholz R, Maier-Hauff K, van Landeghem FKH, Waldoefner N, Teichgraeber U, et al.
606 The effect of thermotherapy using magnetic nanoparticles on rat malignant glioma. Journal of
607 Neuro-Oncology. mai 2006;78(1):7‑14.

608 6. Zhao Q, Wang L, Cheng R, Mao L, Arnold RD, Howerth EW, et al. Magnetic Nanoparticle-Based
609 Hyperthermia for Head & Neck Cancer in Mouse Models. Theranostics. 2012;2(1):113‑21.

610 7. Thiesen B, Jordan A. Clinical applications of magnetic nanoparticles for hyperthermia. International
611 Journal of Hyperthermia. janv 2008;24(6):467‑74.

612 8. Silva AC, Oliveira TR, J. B. Mamani, Malheiros SMF, Malavolta L, Pavon LF, et al. Application of
613 hyperthermia induced by superparamagnetic iron oxide nanoparticles in glioma treatment.
614 International Journal of Nanomedicine. mars 2011;591.

615 9. Fine HA, Dear KB, Loeffler JS, Black PM, Canellos GP. Meta-analysis of radiation therapy with
616 and without adjuvant chemotherapy for malignant gliomas in adults. CANCER-PHILADELPHIA-.
617 1993;71:2585–2585.

618 10. Branquinho LC, Carrião MS, Costa AS, Zufelato N, Sousa MH, Miotto R, et al. Effect of magnetic
619 dipolar interactions on nanoparticle heating efficiency: Implications for cancer hyperthermia.
620 Scientific Reports [Internet]. 7 oct 2013 [cité 1 juill 2016];3. Disponible sur:
621 http://www.nature.com/articles/srep02887

622 11. Johannsen M, Gneveckow U, Eckelt L, Feussner A, WaldÖFner N, Scholz R, et al. Clinical
623 hyperthermia of prostate cancer using magnetic nanoparticles: Presentation of a new interstitial
624 technique. International Journal of Hyperthermia. nov 2005;21(7):637‑47.

625 12. Laurent S, Dutz S, Häfeli UO, Mahmoudi M. Magnetic fluid hyperthermia: Focus on
626 superparamagnetic iron oxide nanoparticles. Advances in Colloid and Interface Science. août
627 2011;166(1‑2):8‑23.

628 13. Frankel RB. The discovery of magnetotactic/magnetosensitive bacteria. Chinese Journal of
629 Oceanology and Limnology. 2009;27(1):1–2.

630 14. Blakemore, Richard. Magnetotactic bacteria. Annual Revew of Microbiology. 1982;36:217‑38.

631 15. Frankel RB, Bazylinski DA. Magnetotaxis: Microbial. eLS. 2002;1‑7.

16. Lin W, Bazylinski DA, Xiao T, Wu L-F, Pan Y. Life with compass: diversity and biogeography of magnetotactic bacteria: Magnetotactic bacterial diversity and biogeography. Environmental Microbiology. sept 2014;16(9):2646‑58.

17. Bazylinski DA, Frankel RB, Heywood BR, Mann S, King JW, Donaghay PL, et al. Controlled Biomineralization of Magnetite (Fe (inf3) O (inf4)) and Greigite (Fe (inf3) S (inf4)) in a Magnetotactic Bacterium. Applied and Environmental Microbiology. 1995;61(9):3232–3239.

18. Schüler D. Genetics and cell biology of magnetosome formation in magnetotactic bacteria. FEMS Microbiology Reviews. juill 2008;32(4):654‑72.

19. Schüler D. Formation of magnetosomes in magnetotactic bacteria. Journal of molecular microbiology and biotechnology. 1999;1(1):79–86.

20. Alphandéry E, Faure S, Seksek O, Guyot F, Chebbi I. Chains of Magnetosomes Extracted from AMB-1 Magnetotactic Bacteria for Application in Alternative Magnetic Field Cancer Therapy. ACS Nano. 23 août 2011;5(8):6279‑96.

21. Xiang L, Wei J, Jianbo S, Guili W, Feng G, Ying L. Purified and sterilized magnetosomes from Magnetospirillum gryphiswaldense MSR-1 were not toxic to mouse fibroblasts in vitro. Letters in Applied Microbiology. juill 2007;45(1):75‑81.

22. Wang X, Wei F, Liu A, Wang L, Wang J-C, Ren L, et al. Cancer stem cell labeling using poly(l-lysine)-modified iron oxide nanoparticles. Biomaterials. mai 2012;33(14):3719‑32.

23. Răcuciu M, Creangă DE, Airinei A. Citric-acid-coated magnetite nanoparticles for biological applications. The European Physical Journal E. oct 2006;21(2):117‑21.

24. Bloemen M, Brullot W, Luong TT, Geukens N, Gils A, Verbiest T. Improved functionalization of oleic acid-coated iron oxide nanoparticles for biomedical applications. Journal of Nanoparticle Research [Internet]. sept 2012 [cité 30 juin 2016];14(9). Disponible sur: http://link.springer.com/10.1007/s11051-012-1100-5

25. Ghosh R, Pradhan L, Devi YP, Meena SS, Tewari R, Kumar A, et al. Induction heating studies of Fe3O4 magnetic nanoparticles capped with oleic acid and polyethylene glycol for hyperthermia. Journal of Materials Chemistry. 2011;21(35):13388‑98.

26. Barrera C, Herrera A, Zayas Y, Rinaldi C. Surface modification of magnetite nanoparticles for biomedical applications. Journal of Magnetism and Magnetic Materials. mai 2009;321(10):1397‑9.

27. Grüttner C, Müller K, Teller J, Westphal F, Foreman A, Ivkov R. Synthesis and antibody conjugation of magnetic nanoparticles with improved specific power absorption rates for alternating magnetic field cancer therapy. Journal of Magnetism and Magnetic Materials. avr 2007;311(1):181‑6.

28. Schultheiss D, Schüler D. Development of a genetic system for Magnetospirillum gryphiswaldense. Archives of microbiology. 2003;179(2):89–94.

29. Zhang Y, Zhang X, Jiang W, Li Y, Li J. Semicontinuous Culture of Magnetospirillum gryphiswaldense MSR-1 Cells in an Autofermentor by Nutrient-Balanced and Isosmotic Feeding Strategies. Applied and Environmental Microbiology. 1 sept 2011;77(17):5851‑6.

30. Philipse AP, Maas D. Magnetic Colloids from Magnetotactic Bacteria: Chain Formation and Colloidal Stability. Langmuir. déc 2002;18(25):9977‑84.

31. Xie J, Liu X, Liu W, Qiu G. Extraction of magnetosome from Acidthiobacillus ferrooxidans. Biomagnetism. 2005;1(3):36–38.

32. Grunberg K, Muller E-C, Otto A, Reszka R, Linder D, Kube M, et al. Biochemical and Proteomic Analysis of the Magnetosome Membrane in Magnetospirillum gryphiswaldense. Applied and Environmental Microbiology. 1 févr 2004;70(2):1040‑50.

33. Magalhães PO, Lopes AM, Mazzola PG, Rangel-Yagui C, Penna TC, Pessoa Jr A. Methods of endotoxin removal from biological preparations: a review. J Pharm Pharm Sci. 2007;10(3):388–404.

34. Babic M, Horák D, Trchová M, Jendelová P, Glogarová K, Lesnỳ P, et al. Poly (L-lysine)-modified iron oxide nanoparticles for stem cell labeling. Bioconjugate chemistry. 2008;19(3):740–750.

35. Kotsmar C, Yoon KY, Yu H, Ryoo SY, Barth J, Shao S, et al. Stable Citrate-Coated Iron Oxide Superparamagnetic Nanoclusters at High Salinity. Ind Eng Chem Res. 15 déc 2010;49(24):12435‑43.

36. Jain TK, Morales MA, Sahoo SK, Leslie-Pelecky DL, Labhasetwar V. Iron Oxide Nanoparticles for Sustained Delivery of Anticancer Agents. Molecular Pharmaceutics. juin 2005;2(3):194‑205.

37. Yang K, Peng H, Wen Y, Li N. Re-examination of characteristic FTIR spectrum of secondary layer in bilayer oleic acid-coated Fe3O4 nanoparticles. Applied Surface Science. mars 2010;256(10):3093‑7.

38. Liu G, Hong RY, Guo L, Li YG, Li HZ. Preparation, characterization and MRI application of carboxymethyl dextran coated magnetic nanoparticles. Applied Surface Science. mai 2011;257(15):6711‑7.

39. Bazylinski DA, Frankel RB. Magnetosome formation in prokaryotes. Nature Reviews Microbiology. mars 2004;2(3):217‑30.

40. Liu R, Liu J, Tong J, Tang T, Kong W-C, Wang X, et al. Heating effect and biocompatibility of bacterial magnetosomes as potential materials used in magnetic fluid hyperthermia. Progress in Natural Science: Materials International. févr 2012;22(1):31‑9.

41. Predoi D, Andronescu E, Radu M, Munteanu MC, Dinischiotu A. Synthesis and characterization of biocompatible maghemite nanoparticles. Digest J Nanom Biostr. 2010;5:779–786.

42. Özdemir Ö, Dunlop DJ. The effect of oxidation on the Verwey transition in magnetite. Geophysical Research Letters. 1993;20(16):1671‑4.

43. Le Fèvre R, Durand-Dubief M, Chebbi I, Mandawala C, Lagroix F, Valet J-P, Maake C, Guyot F, Alphandéry E, Enhanced antitumor efficacy of biocompatible magnetosomes compared with chemically synthesized nanoparticles for the magnetic hyperthermia treatment of murine GL-261 glioblastoma.Manuscript in preparation.[When N-PLL and IONP were administered intratumorally to mice bearing GL-261 tumors and were then exposed 11 to 15 times to an alternating magnetic field of 198 kHz and 25 mT for 30 minutes, it led to 50% and 20% of mice fully cured with N-PLL and IONP, respectively.].

44. Alphandéry E, Ding Y, Ngo AT, Wang ZL, Wu LF, Pileni MP. Assemblies of Aligned Magnetotactic Bacteria and Extracted Magnetosomes: What Is the Main Factor Responsible for the Magnetic Anisotropy? ACS Nano. 23 juin 2009;3(6):1539‑47.

45. Abbas M, Islam MN, Rao BP, Abdel-Hamed MO, Kim C. Facile one-pot chemical approach for synthesis of monodisperse chain-like superparamagnetic maghemite (γ-Fe2O3) nanoparticles. Journal of Industrial and Engineering Chemistry. nov 2015;31:43‑6.

46. Chen ZP, Zhang Y, Zhang S, Xia JG, Liu JW, Xu K, et al. Preparation and characterization of water-soluble monodisperse magnetic iron oxide nanoparticles via surface double-exchange with DMSA. Colloids and Surfaces A: Physicochemical and Engineering Aspects. mars 2008;316(1‑3):210‑6.

47. ISO 10993-12:2012(en), Biological evaluation of medical devices — Part 12: Sample preparation and reference materials [Internet]. [cited 2016 Oct 26]. Available from: https://www.iso.org/obp/ui/#iso:std:53468:en. To estimate that 22 µg/mL corresponds to 6 cm2 per ml, we use the formula: 22 µg/mL = 6÷ (2.2 10 15×12,15 10-11), where 2.2 × 1015 per gram is the number of magnetosomes per gram and 12.15×10-11 cm2 is the specific magnetosome surface area.

48. Panasci L, Jean-Claude BJ, Vosilescu D, Mustafa A, Damian S, Damian Z, et al. Sensitization to doxorubicin resistance in breast cancer cell lines by tamoxifen and megestrol acetate. Biochemical Pharmacology. 1996;52(7):1097‑102.

49. Rantanen V, Grénman S, Kulmala J, Grénman R. Comparative evaluation of cisplatin and carboplatin sensitivity in endometrial adenocarcinoma cell lines. British journal of cancer. 1994;69(3):482.

50. de Sousa ME, Fernández van Raap MB, Rivas PC, Mendoza Zélis P, Girardin P, Pasquevich GA, et al. Stability and Relaxation Mechanisms of Citric Acid Coated Magnetite Nanoparticles for Magnetic Hyperthermia. The Journal of Physical Chemistry C. 14 mars 2013;117(10):5436‑45.

51. Wilhelm C, Billotey C, Roger J, Pons JN, Bacri J-C, Gazeau F. Intracellular uptake of anionic superparamagnetic nanoparticles as a function of their surface coating. Biomaterials. mars 2003;24(6):1001‑11.

52. Rabin Y. Is intracellular hyperthermia superior to extracellular hyperthermia in the thermal sense? International Journal of Hyperthermia. 1 janv 2002;18(3):194‑202.

53. Jadhav NV, Prasad AI, Kumar A, Mishra R, Dhara S, Babu KR, et al. Synthesis of oleic acid functionalized Fe3O4 magnetic nanoparticles and studying their interaction with tumor cells for potential hyperthermia applications. Colloids and Surfaces B: Biointerfaces. août 2013;108:158‑68.

54. Alphandéry E, Idbaih A, Adam C, Delattre JY, Schmitt C, Guyot F, Chebbi I, Full intracranial U87-Luc tumor disappearance in 100% of mice bearing these tumors using nonpyrogenic magnetosome minerals coated with poly-L-lysine heated under the application of an alternating magnetic field. Manuscript in preparation.

FIGURES and TABLE:

Figure 1: TEM images of whole magnetotactic bacteria, IONP, uncoated and coated magnetosome minerals. (a), Transmission electron microscopy images of a magnetotactic bacterium *Magnetospirillum gryphiswaldense* used in this study and containing a chain of magnetosomes; (b), chemical nanoparticles IONP; (c), magnetosome minerals without coating, N; (d,e), magnetosome minerals coated with either poly-L-lysine, N-PLL; (f,g), citric acid, N-CA; (h,i), oleic acid, N-OA; (j,k), carboxy-methyl-dextran, N-CMD.

Figure 2: Physicochemical properties of uncoated and coated magnetosome minerals.
(a), Size distribution of uncoated magnetosome minerals, measured over 500 magnetosomes. (b), Weight percentage of carbon and nitrogen in the different nanoparticles, measured by CHNS. (c) and (d), Variation with time of the absorbance, measured at 480 nm, of suspensions containing of 1mg/mL in iron of uncoated, coated magnetosome minerals and IONP. (e) and (f), Variation of Zeta potential of uncoated, coated magnetosome minerals and IONP as a function of pH. These results were obtained from triplicates. The error bars represent standard deviations (SD°).

Figure 3: FTIR spectra of IONP, uncoated and coated magnetosome minerals.
Fourier transform infrared, FT-IR spectra of, (a), lyophilized uncoated magnetosome minerals, N; (b), lyophilized IONP; (c), lyophilized magnetosome minerals coated with poly-L-lysine, N-PLL; (d), with citric acid, N-CA; (e), oleic acid, N-OA; (f), carboxy-methyl-dextran, N-CMD.

Figure 4: Percentages of 3T3, RG2, and GL-261 cell inhibition in the presence of IONP, uncoated and coated magnetosome minerals.
(a), Percentage of 3T3 cell inhibition after 24 hours of 3T3 cell incubation with various concentrations of uncoated, coated magnetosome minerals and IONP; (b), Percentage of GL-261 cells inhibition after 24 hours of 3T3 cell incubation with various concentrations of uncoated, coated magnetosome minerals

and IONP; (c), Percentage of GL-261 cell inhibition after 72 hours of 3T3 cell incubation with various concentrations of uncoated, coated magnetosome minerals and IONP.

Figure 5: Heating properties of IONP, uncoated and coated magnetosome minerals, in the presence of GL-261 cells and AMF application.

(a), Variation of temperature of GL-261 cells brought into contact with 1mg/mL of uncoated and coated magnetosome minerals and exposed (or not) to an alternating magnetic field of frequency 198 kHz and strength H = 34 mT. (b), Spatial temperature distribution of concentration 1 mg /ml of N, N-PLL, N-CA, N-OA, N-CMD, and IONP mixed with GL-261cells and exposed to an alternating magnetic field of frequency 198 kHz and average field strength of 34 mT during 30 min.

Figure 6: Percentage of cell inhibition and quantity of heat produced by the various nanoparticles under AMF application.

(a), Flow cytometry results showing the percentage of living GL-261 cells treated with or without AMF with uncoated, coated magnetosome minerals and IONP, (b), Spatial temperature distribution within the Petri dish of N, N-PLL, N-CA, N-OA, N-CMD, and IONP mixed with GL-261 cells and exposed to an alternating magnetic field of frequency 198 kHz and average field strength adjusted between 34 and 47 mT to maintain the temperature of cells mixed with the nanoparticles at 45 °C during 30 min.

Figure 7: **Quantity of iron coming from the various nanoparticles internalized in cells or localized at cell surface after and before AMF application.** Quantity of iron per cell (pg) for cells treated with or without AMF.

Table 1: $\Delta T/\delta t$ estimated in °C/s; specific absorption rate, estimated in Watt per gram of nanoparticle in iron, temperature variation, and percentage of heated area at 43-46°C for uncoated, coated magnetosome minerals and IONP brought into contact with GL-261 cells and exposed to an alternating magnetic field of 198 kHz and strength 32 mT applied during 30 minutes.

791 **Table 2**: Percentage of heated area at 43-46°C for uncoated, coated magnetosome minerals and IONP
792 mixed with GL-261 cells and exposed to an alternating magnetic field of 198 kHz and strength of 32 mT
793 applied during 30 minutes.

794

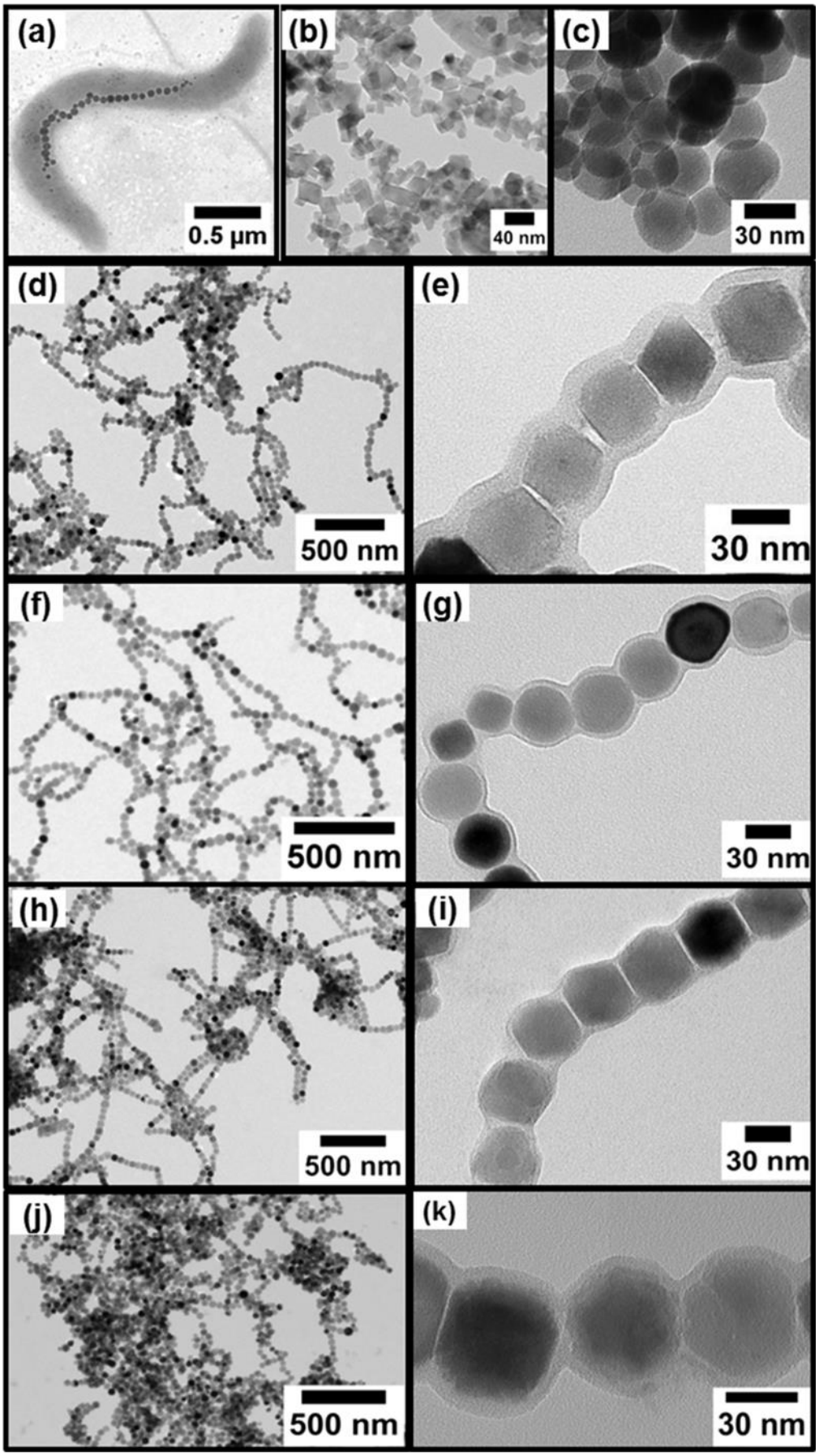
(a)
0.5 µm
(b)
40 nm
(c)
30 nm
(d)
500 nm
(e)
30 nm
(f)
500 nm
(g)
30 nm
(h)
500 nm
(i)
30 nm
(j)
500 nm
(k)
30 nm

Figure 1

795

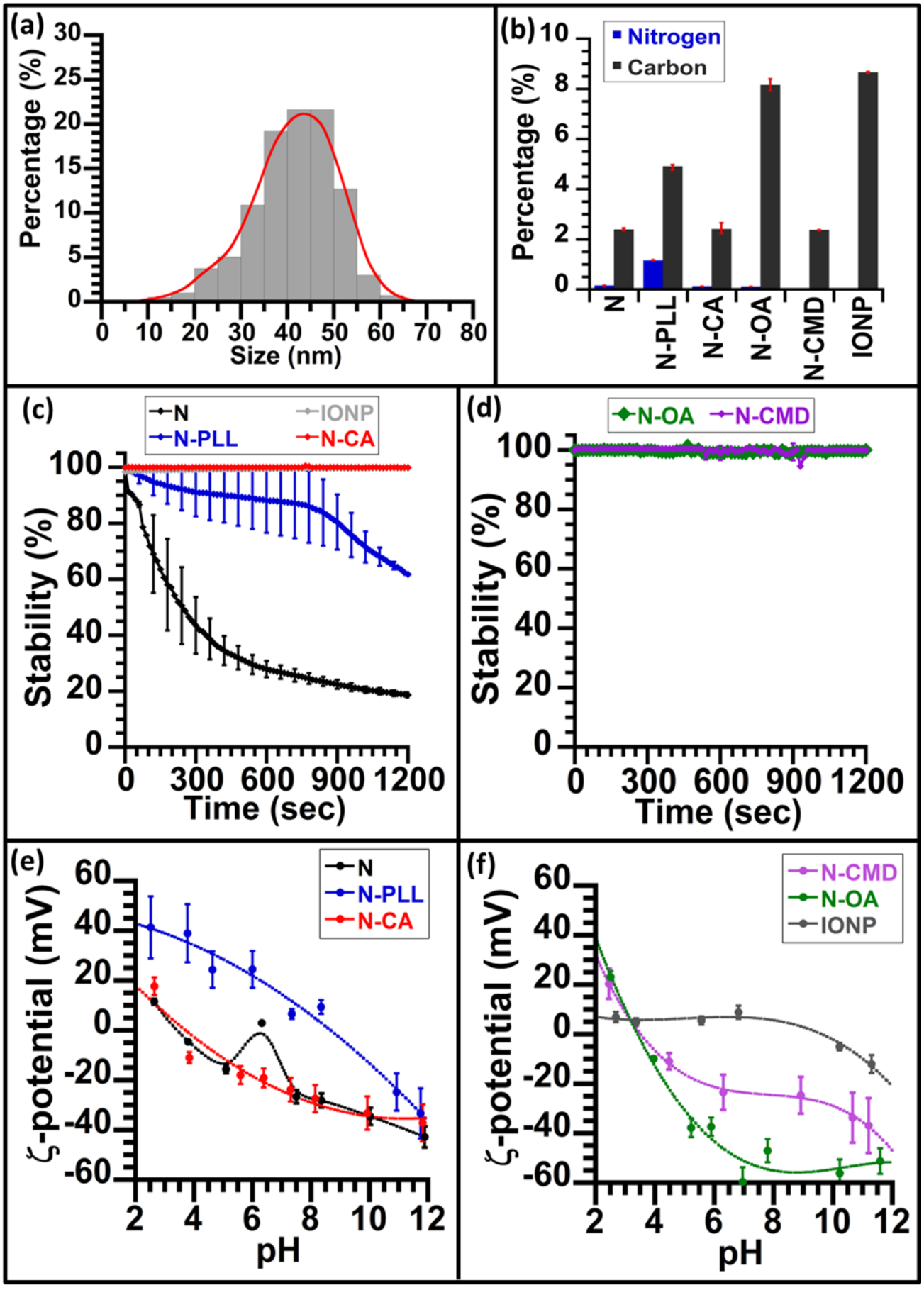
(a)
Percentage (%)
Size (nm)
(b)
Nitrogen
Carbon
Percentage (%)
N
N-PLL
N-CA
N-OA
N-CMD
IONP
(c)
N
N-PLL
IONP
N-CA
Stability (%)
Time (sec)
(d)
N-OA
N-CMD
Stability (%)
Time (sec)
(e)
N
N-PLL
N-CA
ζ-potential (mV)
pH
(f)
N-CMD
N-OA
IONP
ζ-potential (mV)
pH

Figure 2

796

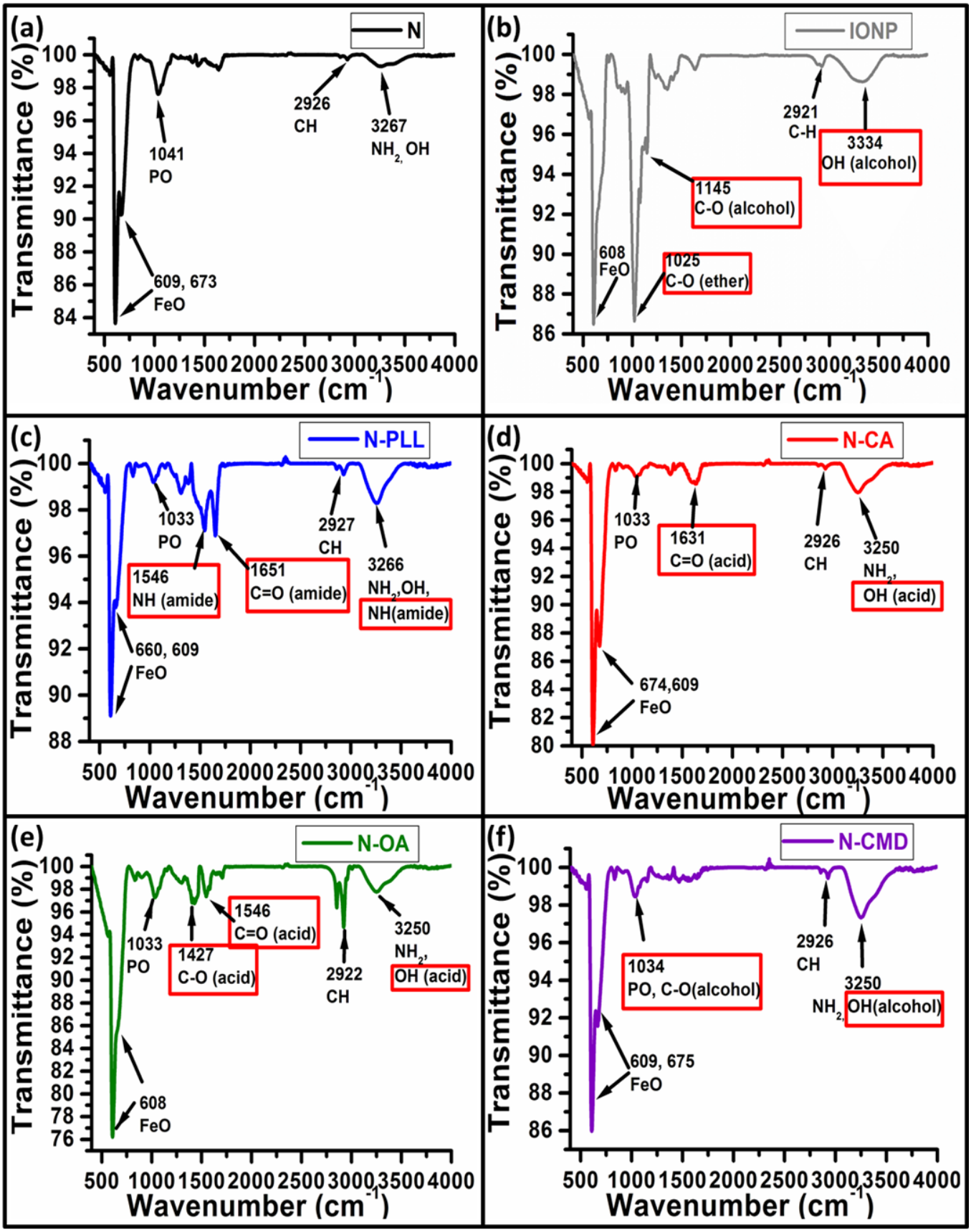
(a)
N
Transmittance (%)
Wavenumber (cm-1)
1041
PO
2926
CH
3267
NH2, OH
609, 673
FeO
(b)
IONP
2921
C-H
3334
OH (alcohol)
1145
C-O (alcohol)
608
FeO
1025
C-O (ether)
(c)
N-PLL
1033
PO
2927
CH
3266
NH2,OH,
NH(amide)
1546
NH (amide)
1651
C=O (amide)
660, 609
FeO
(d)
N-CA
1033
PO
1631
C=O (acid)
2926
CH
3250
NH2,
OH (acid)
674,609
FeO
(e)
N-OA
1033
PO
1427
C-O (acid)
1546
C=O (acid)
2922
CH
3250
NH2,
OH (acid)
608
FeO
(f)
N-CMD
1034
PO, C-O(alcohol)
2926
CH
3250
NH2, OH(alcohol)
609, 675
FeO

Figure 3

797

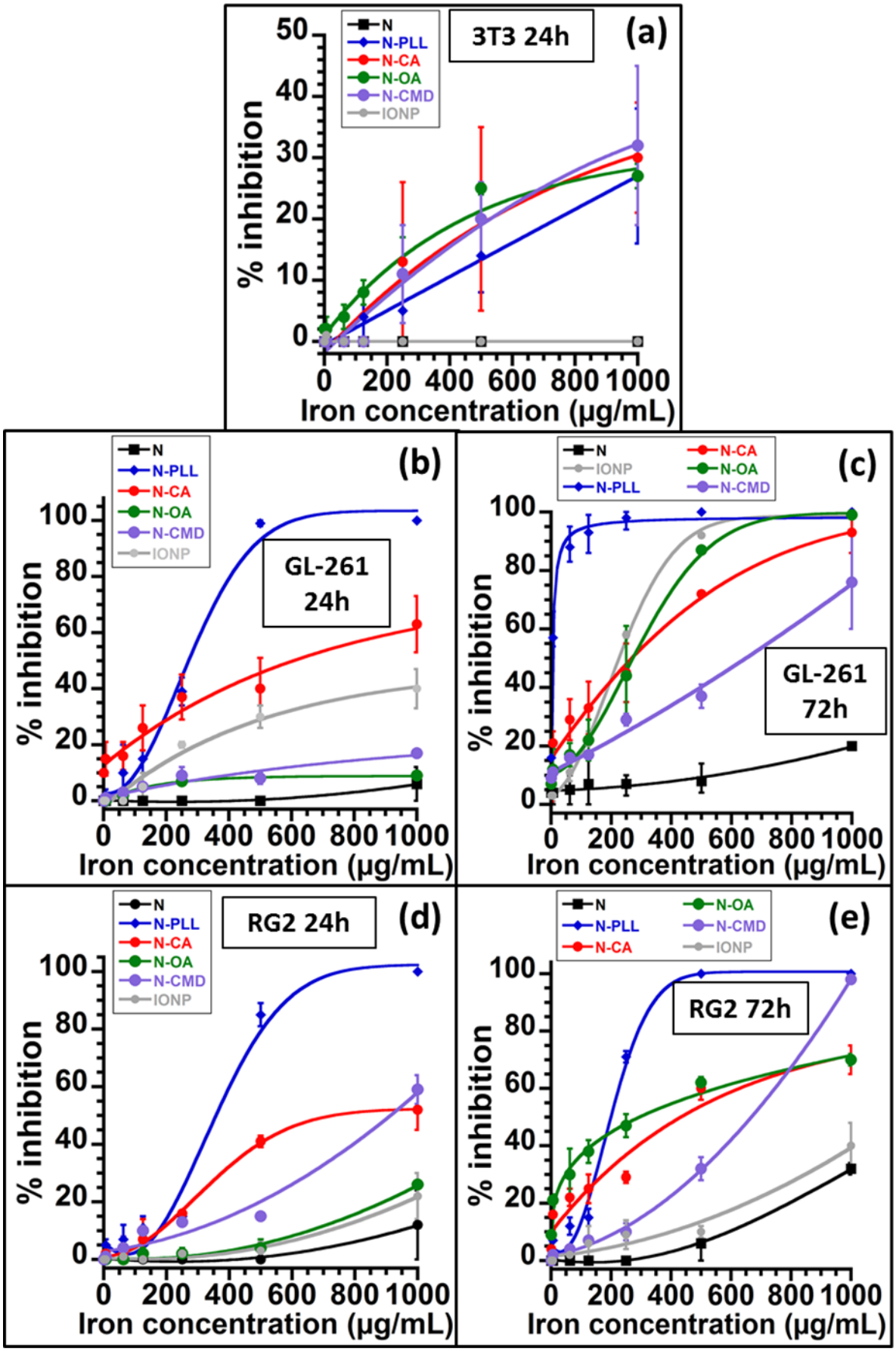
(a)
3T3 24h
N
N-PLL
N-CA
N-OA
N-CMD
IONP
% inhibition
Iron concentration (µg/mL)
(b)
GL-261 24h
(c)
GL-261 72h
(d)
RG2 24h
(e)
RG2 72h

Figure 4

798

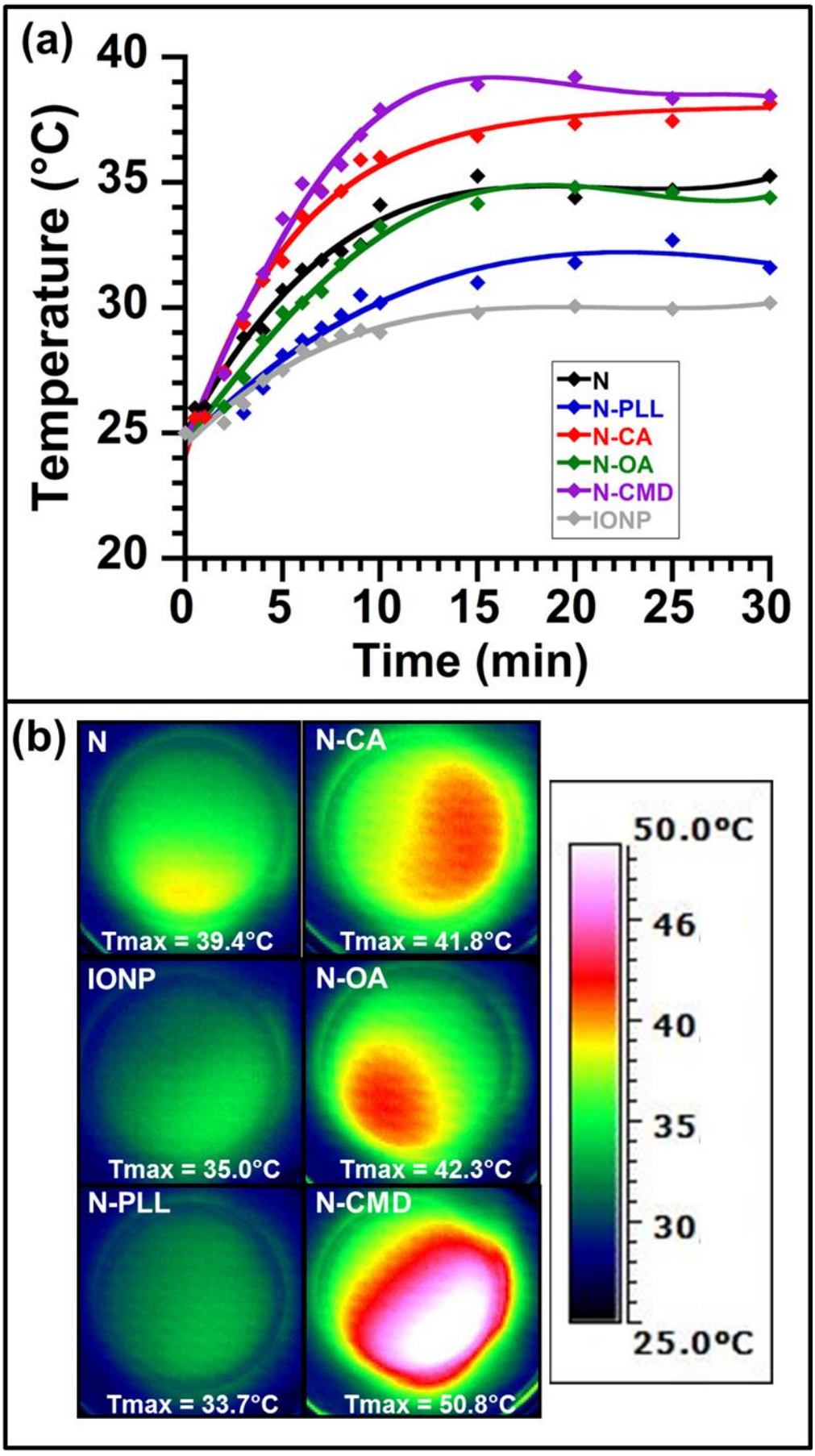
(a)
Temperature (°C)
40
35
30
25
20
0
5
10
15
20
25
30
Time (min)
N
N-PLL
N-CA
N-OA
N-CMD
IONP
(b)
N
Tmax = 39.4°C
N-CA
Tmax = 41.8°C
IONP
Tmax = 35.0°C
N-OA
Tmax = 42.3°C
N-PLL
Tmax = 33.7°C
N-CMD
Tmax = 50.8°C
50.0°C
46
40
35
30
25.0°C

Figure 5

799

	ΔT/δt (°C/s)	SAR (W/g of iron)	Percentage of heated area at 43- 46 °C (%)
N	2.30E-02	96	0.0
IONP	1.80E-02	73	0.0
N-PLL	2.10E-02	89	0.0
N-CA	3.40E-02	141	12.7
N-OA	2.40E-02	100	12.4
N-CMD	4.70E-02	196	90.1

Table 1

800

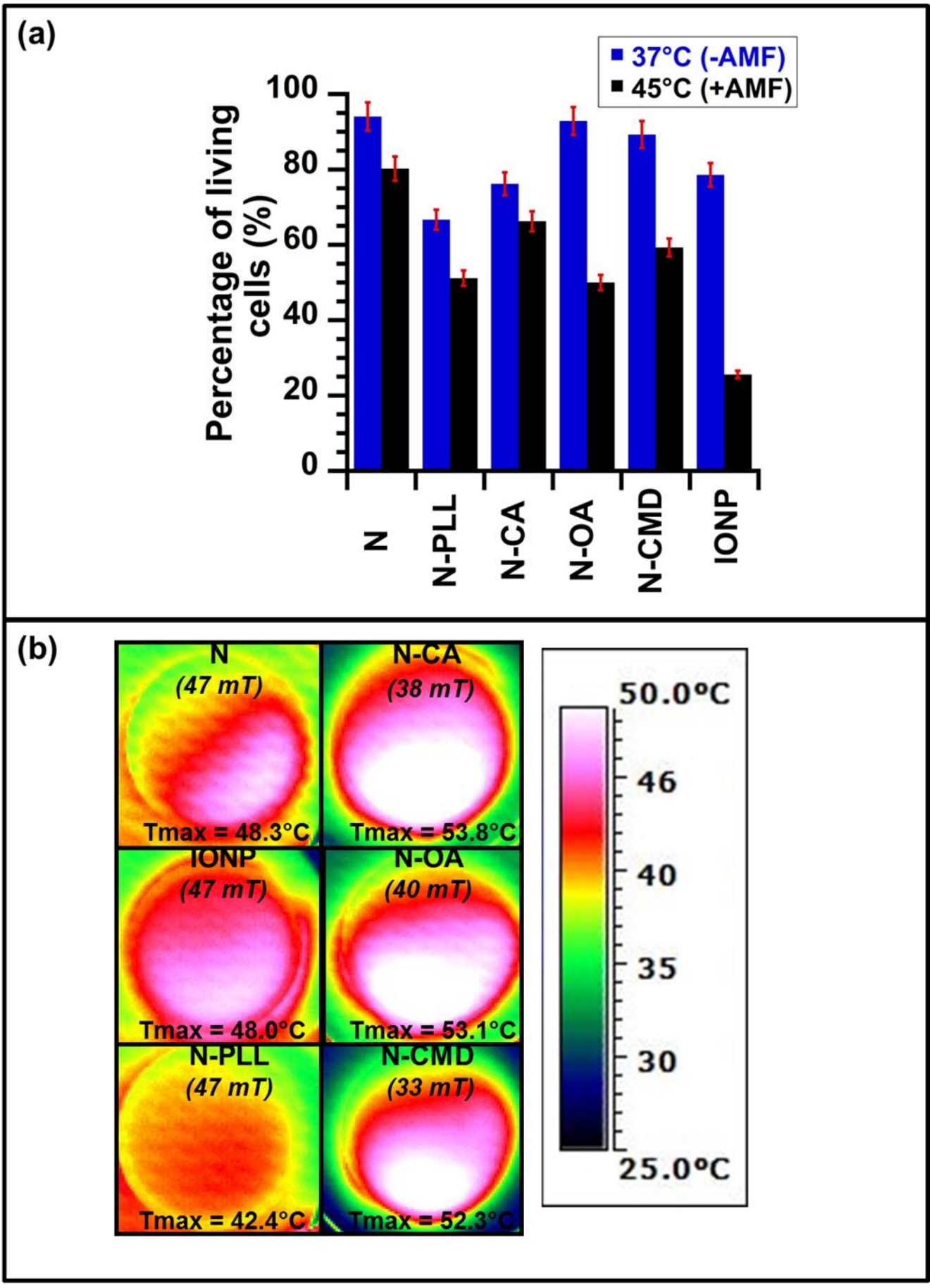
(a)
37°C (-AMF)
45°C (+AMF)
Percentage of living cells (%)
100
80
60
40
20
0
N
N-PLL
N-CA
N-OA
N-CMD
IONP
(b)
N
(47 mT)
Tmax = 48.3°C
N-CA
(38 mT)
Tmax = 53.8°C
IONP
(47 mT)
Tmax = 48.0°C
N-OA
(40 mT)
Tmax = 53.1°C
N-PLL
(47 mT)
Tmax = 42.4°C
N-CMD
(33 mT)
Tmax = 52.3°C
50.0°C
46
40
35
30
25.0°C

Figure 6

801

	Percentage of heated area at 43- 46 °C (%)
N	89.4
IONP	100.0
N-PLL	32.0
N-CA	100.0
N-OA	100.0
N-CMD	100.0

Table 2

802

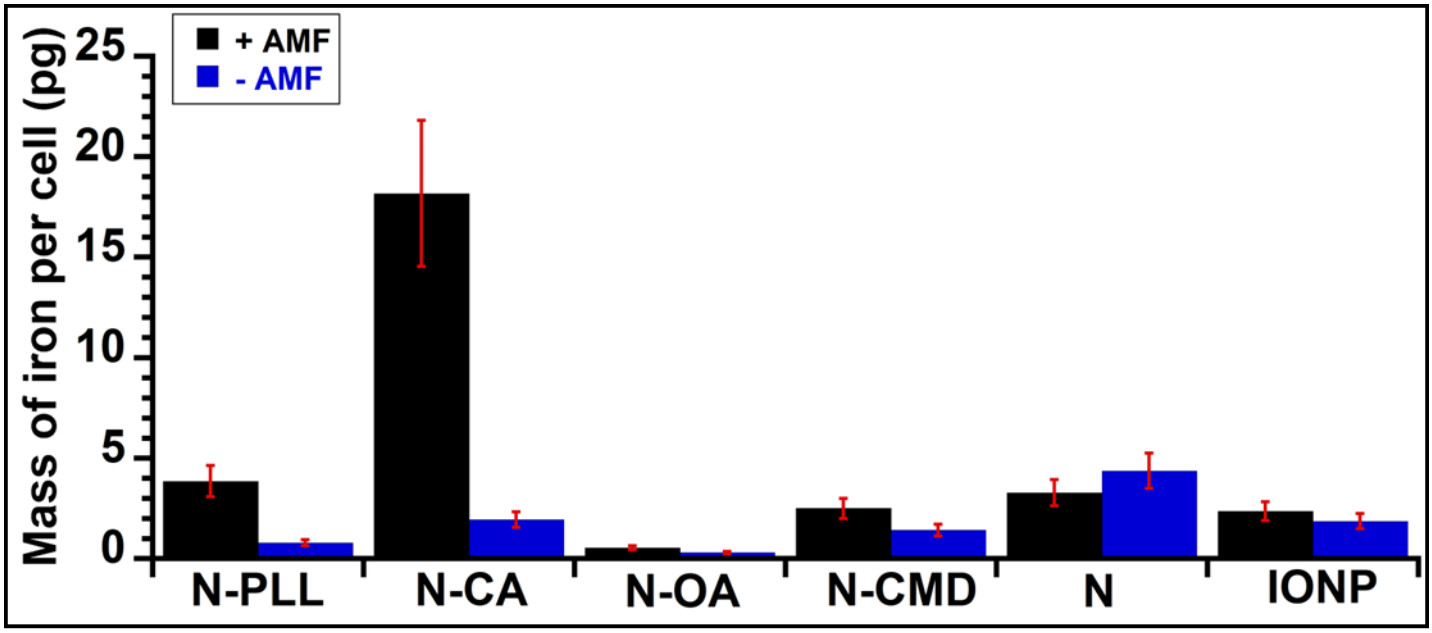

Figure 7

803

804

805

806

807